

NANO-CRYSTALLOGRAPHY OF INDIVIDUAL CARBON NANOTUBES

N. Božović^{1,2}, J. Misewich^{1,3} and I. Božović^{1*}

¹*Brookhaven National Laboratory, Upton, New York 11973, USA*

²*San Jose State University, San Jose, California, USA*

³*Columbia University, New York, USA*

1. Introduction

Commissioning of ever-better synchrotron sources in the last couple decades has spurred rapid progress in x-ray diffraction (XRD) crystallography. Brookhaven National Laboratory expects to start building in near future the next-generation machine, the Second National Synchrotron Light Source. NSLS II is projected to deliver a beam of $10^{13} - 10^{14}$ photons/sec at the brightness of 10^{21} photons/sec/0.1% BW/mm²/m² -- an order-of-magnitude brighter than any existing synchrotron, in particular in the hard x-ray region. It is expected to achieve 1 meV energy resolution and 1 nm spatial resolution.¹ The later should enable nano-crystallography – XRD study of individual nano-particles.

The commissioning of NSLS II will take some time -- the plan is to start construction in 2007 and be operational by 2013. Nevertheless, it is timely to ask now what one should expect to observe. Nano-particles are excruciatingly small by XRD standards, and the critics have raised concerns whether (i) a reasonable counting statistics could be reached within a realistic accumulation time, and whether (ii) the nano-diffractograms

would carry any useful information or would be completely blurred because of small-size broadening.

Here we address these questions by extensive numerical simulations of XRD patterns from a variety of carbon nanotubes (CNTs). The motivation for this particular choice is as follows. Carbon nanotubes (CNTs) have been at focus of worldwide research lately. Their most interesting electronic properties – metallic or semiconducting transport, electro-luminescence, photo-conductivity, optical dichroism, etc. - depend sensitively on the CNT structure, i.e., the type (armchair, zig-zag, or chiral) and radius. They are also influenced by the presence of structural defects or impurities such as adatoms or catalyst residue. Therefore, to understand the electronic properties of a single CNT, we first and foremost need detailed information on its atomic structure. However, the traditional XRD has been hampered by the lack of macroscopic CNT crystals - mono-disperse and ordered samples in which all the CNTs would be the same and in a perfect crystalline register. Individual CNTs have been imaged by transmission electron microscopy (TEM) – indeed, this is how CNTs were discovered – or by scanning tunneling microscopy (STM), but unraveling the CNT structure in this way is tedious, time-consuming, and the resolution is limited to about 1 Å.

Here we show that with the projected NSLS II brilliance and beam focus, one should be able to determine unambiguously the CNT type, radius, and orientation within a reasonable accumulation time - on the scale of minutes. Next, we have also studied CNTs functionalized by insertion or adsorption of foreign atoms, and we show that the presence of even a single adsorbed atom can be discerned in simulated XRD patterns.

2. The model and equations

The model we have used is illustrated in Fig. 1a. A single CNT is illuminated by a perpendicular x-ray polarized parallel to the tube. (In reality, this axis will be horizontal.) The diffraction is recorded by a 512x512 pixel detector array, positioned at a distance $d = 20$ cm; the pixel area is $200 \times 200 \mu\text{m}^2$. (These are quite realistic values; ten times higher resolution is feasible today.) The number of photons N reaching the pixel detector at \vec{R} is given by:

$$N(\vec{R}) = I_{sc} \Delta t = I_0 \Delta t (A_p / A_0) (r_0/R)^2 P(Q) [(\sum_j f_j \cos \phi_j)^2 + (\sum_j f_j \sin \phi_j)^2] \quad (1)$$

where I_{sc} is the scattered intensity (number of photons per second impinging on the detector); Δt is the accumulation time; I_0 is the incident intensity (number of photons per second impinging on the illuminated area A_0 of the CNT under study); $A_p = R^2 \Delta\Omega$ is the (effective) area of the detector and $\Delta\Omega$ is the solid angle that it subtends; $r_0 = 2.8 \times 10^{-6}$ nm is the classic (Thomson) electron radius; the pixel position is specified by $\vec{R} = (X, Y, Z) = (d, mb, nb)$ where $m, n = -215, \dots, 216$ and $b = 200 \mu\text{m}$; $P(Q) = 1 - (\mathbf{e}_o \cdot \mathbf{s}')^2$ is the polarization factor, \mathbf{e}_o is the direction of polarization of synchrotron light, $\mathbf{s}' = \vec{R}/R$ is the direction of scattered light; $f_j(Q)$ is the atomic scattering (form) factor of the atom at \mathbf{r}_j (such form factors have been calculated *ab initio* and tabulated in the literature); $\mathbf{Q} = \mathbf{k} - \mathbf{k}'$ is the momentum transfer where \mathbf{k} and \mathbf{k}' are the momentum of the incident and the scattered x-ray photon respectively, and $\phi_j = (\mathbf{Q}, \mathbf{r}_j)$. Values representative of the ex-

pected NSLS II performance and of a single CNT are $I_0 \sim 10^{11}$ photons per second and $A_0 \sim 10^{-12}$ cm².

The computations were performed on the Galaxy parallel computer (256-processor cluster) at Computational Science Center in BNL. In the present simulations, we have chosen the photon accumulation time $\Delta t = 1$ h, which turned to be sufficiently long to achieve the statistical error (shot noise) $\delta N = \sqrt{N}$ less than 1% for the smallest CNT under study. Indeed, the noise is even smaller for larger CNTs. Hence, it should be possible to acquire diffractograms of reasonable quality within minutes. Note that in these simulations we have ignored Compton scattering and the thermal effects (Debye-Waller factor and diffuse thermal scattering) since these only give rise to a weak and constant diffuse background. These effects are negligible compared to the extreme diffraction peak broadening due to tiny lateral dimensions of CNTs. For the same reason, we have neglected unavoidable but small beam divergence (~ 1 mrad).

3 Results

In Fig. 1b we show a typical calculated XRD pattern; the total count is shown (color-coded) on a log scale, because the central peak is typically an order-of-magnitude stronger than the nearest peak. This particular pattern corresponds to a (3,3) CNT of the diameter 0.4 nm, the smallest-diameter CNT synthesized so far. The gross features of the pattern - existence of several horizontal 'streaks' with some finer structure - can be understood readily. In the Z direction, i.e., along the long CNT axis, the diffraction is sharply peaked, because our 25 nm-long model has 100 unit cells and the expected

broadening is small. From the simple Scherrer formula: $B(2\theta) = 0.94 \lambda / L \cos\theta$ (where $B(2\theta)$ is the full-width at half-maximum, measured in radians, θ is the scattering angle; and L is the crystallite size) one would indeed expect the diffraction peaks to be broadened by about 0.1° which here corresponds to about two pixels only. The Z-axis position of the streaks is determined by the Bragg diffraction condition, $n\lambda = d^* \sin 2\theta$; the three streaks seen in Fig. 1 b correspond to $n = -1$, $n = 0$, and $n = 1$, respectively. In the Y direction (i.e., perpendicular to the long CNT axis), the features are roughly 50 times broader, as indeed expected since the diameter of the nanotube under study is about 0.5 nm; this is why we see 'streaks' rather than spots. The slight curvature of streaks comes from our choice of a flat screen; if the screen were cylindrical and coaxial with the CNT, the streaks would be strictly horizontal. For this particular diffractogram, we have oriented the CNT in such a way that the xz plane coincides with one of its 6 vertical mirror symmetry planes (σ_v), while the xy plane coincides with a horizontal mirror symmetry plane (σ_h). In this case, the XRD image is indeed symmetric itself with respect to both σ_h and σ_v .

In Fig. 2a-d, we examine what happens when the same CNT is rotated counterclockwise around the z-axis, in the increments of 10° . The effect of rotation is clearly discernible; it is particularly noticeable for $\phi = 10^\circ$ and $\phi = 20^\circ$ that the diffractogram has lost the original σ_v symmetry. It is restored again for $\phi = 30^\circ$, as expected since the line-group $L6_3/mcm$ of this nanotube contains 6 vertical symmetry planes, one at every 30° .

In Fig. 3 a-d, we show how a change in the CNT diameter is reflected in XRD patterns, by comparing the (3,3), (4,4), (5,5) and (10,10) CNTs with the diameters $D = 0.5$ nm, D

= 0.6 nm, $D = 0.7$ nm, and $D = 1.4$ nm, respectively. As expected, the vertical periodicity of the XRD pattern is unaffected, since the c_0 lattice constant stays the same. However, the lateral modulation of the streaks changes dramatically: the number of peaks increases and they get narrower. From such a diffractogram, one can easily determine the tube diameter: $D = (1/n\lambda) * [1 + (d/Y_m)^2]^{1/2}$, where Y_m is the position of the m -th lateral peak. It is thus sufficient to simply count the number of lateral peaks. Another, experimentally more involved, way would be to rotate the tube along the z -axis and count the number of vertical mirror symmetry planes: the line groups of these four CNTs are $L6_3/mcm$, $L8_4/mcm$, $L10_5/mcm$, and $L20_{10}/mcm$, which corresponds to having one vertical mirror-symmetry plane at every $2\pi/6$, $2\pi/8$, $2\pi/10$ and $2\pi/20$, respectively.

In Fig. 4 a-c, we are comparing the (3,3) armchair, the (5,0) zig-zag, and the (4,2) helical tube - i.e., we vary the CNT type while keeping the tube diameter (almost) constant at about 0.4 nm. Again, if one would rotate these CNTs, one could unambiguously determine the symmetry elements; the respective line groups are $L6_3/mcm$, $L10_5/mcm$, $L28_{22}22$, and $L28_622$. However, the most distinctive feature in Figs. 4a-c is the periodicity along the z -axis, corresponding in real space to the translational periods $c_0 = 0.25$ nm, $c_0 = 0.43$ nm, and $c_0 = 1.14$ nm; this is sufficient to clearly differentiate among (3,3), (5,0) and (4,2) CNTs, respectively.

In our last panel, Fig. 5a-e we illustrate the changes in the XRD pattern caused by addition of a *single* atom of gold adsorbed to the surface of a CNT. In Fig 5a, for comparison we show again the XRD pattern from a pristine (4,2) CNT. The pattern in Fig. 5b is from the same CNT but with a single Au atom attached to its side, at $z=0$. The remain-

ing three diffractograms also correspond to the same CNT with a single Au adatom, but attached at different locations. In Fig. 3c, it is also attached to the side, but shifted half-the-unit-cell upwards; in Fig. 5d it is placed at the top of the tube, and in Fig. 5e it is again attached to the side but near the top of the tube. Note that the pattern is noticeably sensitive to the presence of a single adatom, and even to its position on the nanotube surface.

4. Discussion and conclusions

By numerical simulations, we have shown that with the next-generation synchrotron sources such as the anticipated NSLS II one should be able to record within minutes an XRD pattern of a single CNT and from it identify its type, diameter, and orientation. Even more exciting, in calculated diffractograms we can discern signatures of presence of a single adatom and even locate its position. This is pushing XRD to the ultimate limit of 'seeing' individual atoms. For these reasons, we feel hopeful that NSLS II may indeed open a new field, nano-crystallography. Actually, it may already be possible to test some of our conclusions by pilot experiments on one of the currently brightest hard-x-ray sources such as the Advanced Light Source at Argonne or the Spring-8 synchrotron in Hyogo, Japan.

Finally, note that it would be straightforward to apply the present approach to treat various structural defects in CNTs, other adatoms, multiple adatoms, foreign atoms (Cu, Co, Ga,...) or small molecules (e.g. buckyballs) inserted into a CNT, as well as other non-carbon nanotubes such as BN, MgB₂,... that have already been synthesized.

Acknowledgement. We are grateful to N. D'Imperio and R. Sundling for technical help and to C. C. Kao, B. Ocko, and Z. Radovic for useful discussion

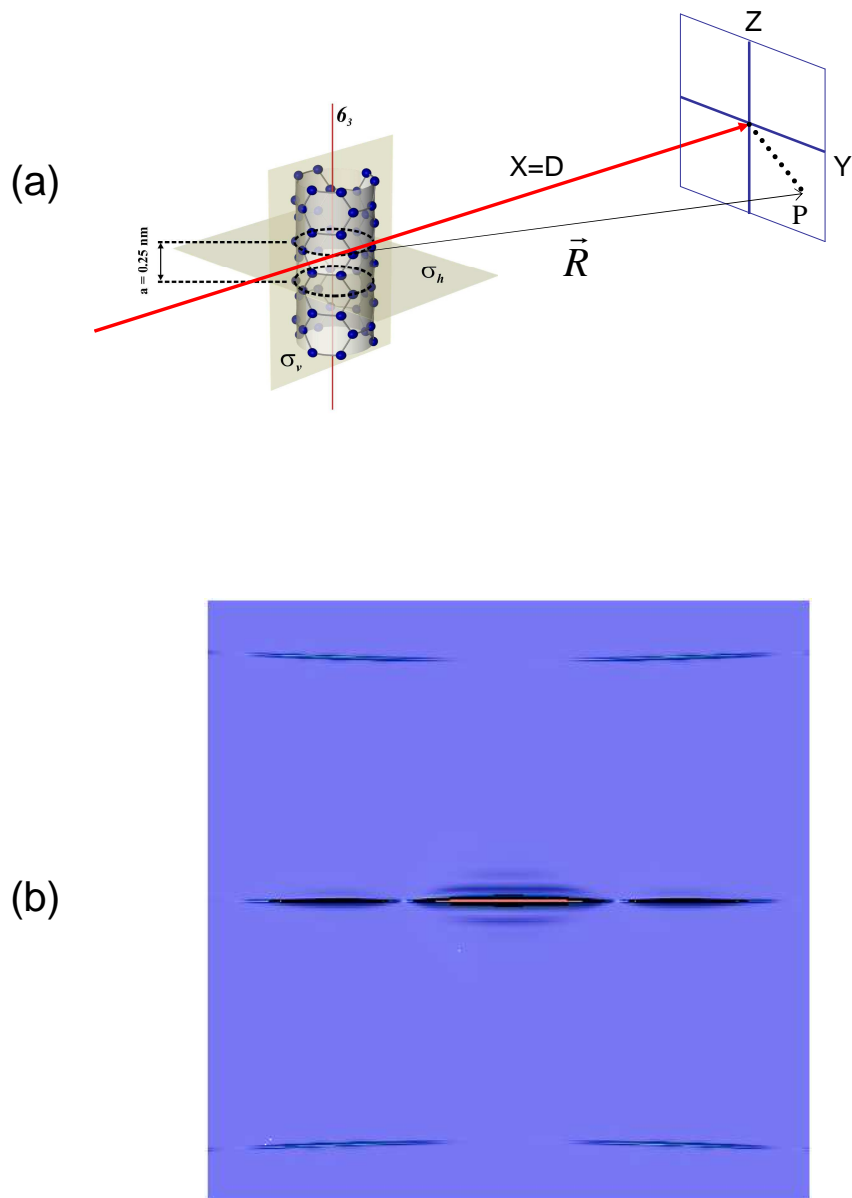


Figure 1. (a) A typical model used in this paper: a single (3,3) armchair carbon nanotube is illuminated by an x-ray beam and the diffraction is recorded on a flat screen. (b) The corresponding XRD pattern (log scale, color-coded).

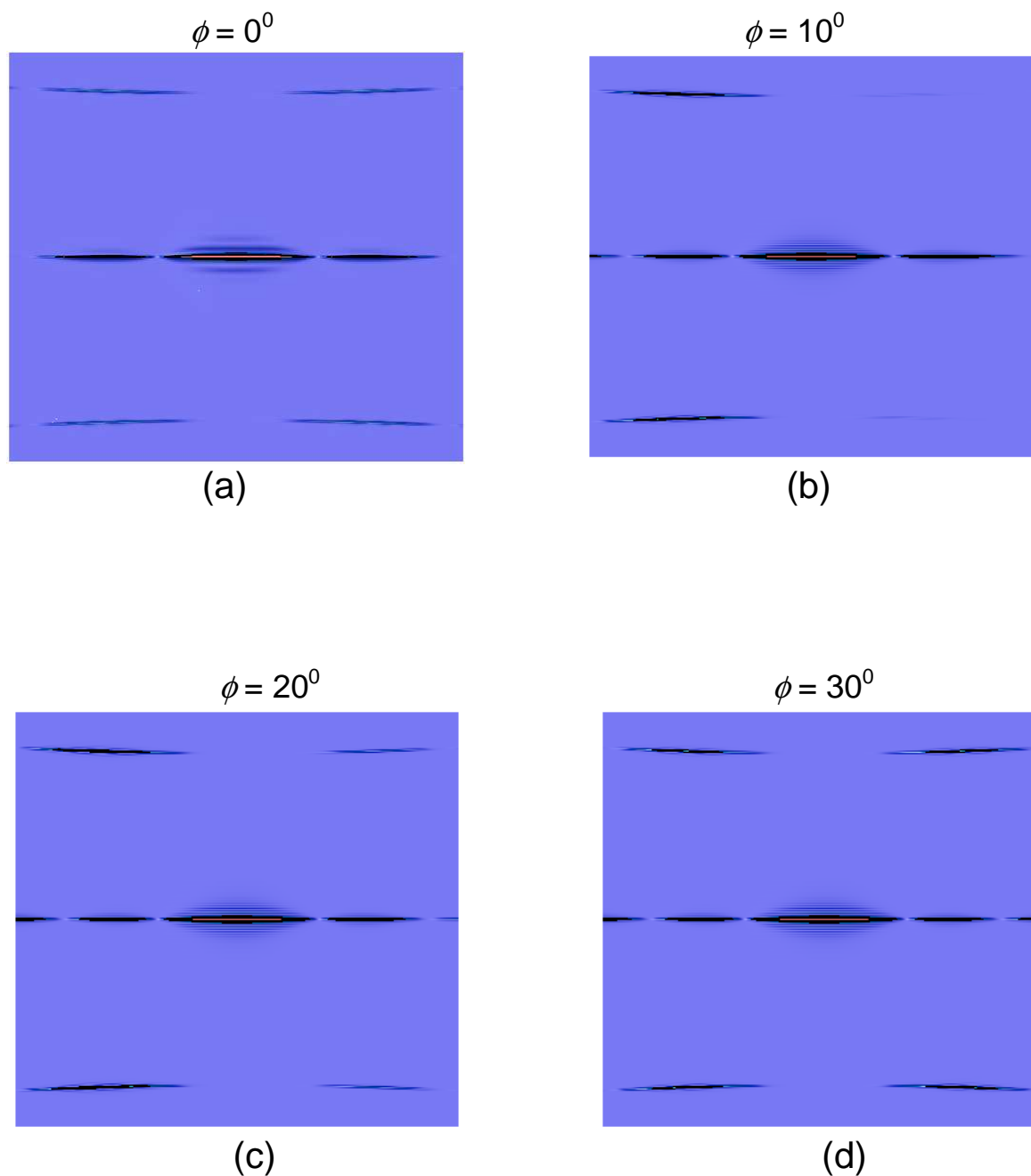


Figure 2. Calculated XRD patterns for the (3,3) armchair CNT, as a function of the relative orientation with respect to the incoming x-ray beam: (a) the beam is parallel to a vertical symmetry plane, $\phi = 0^\circ$; (b) the same CNT rotated by $\phi = 10^\circ$ around the vertical axis, (c) $\phi = 20^\circ$, (d) $\phi = 30^\circ$.

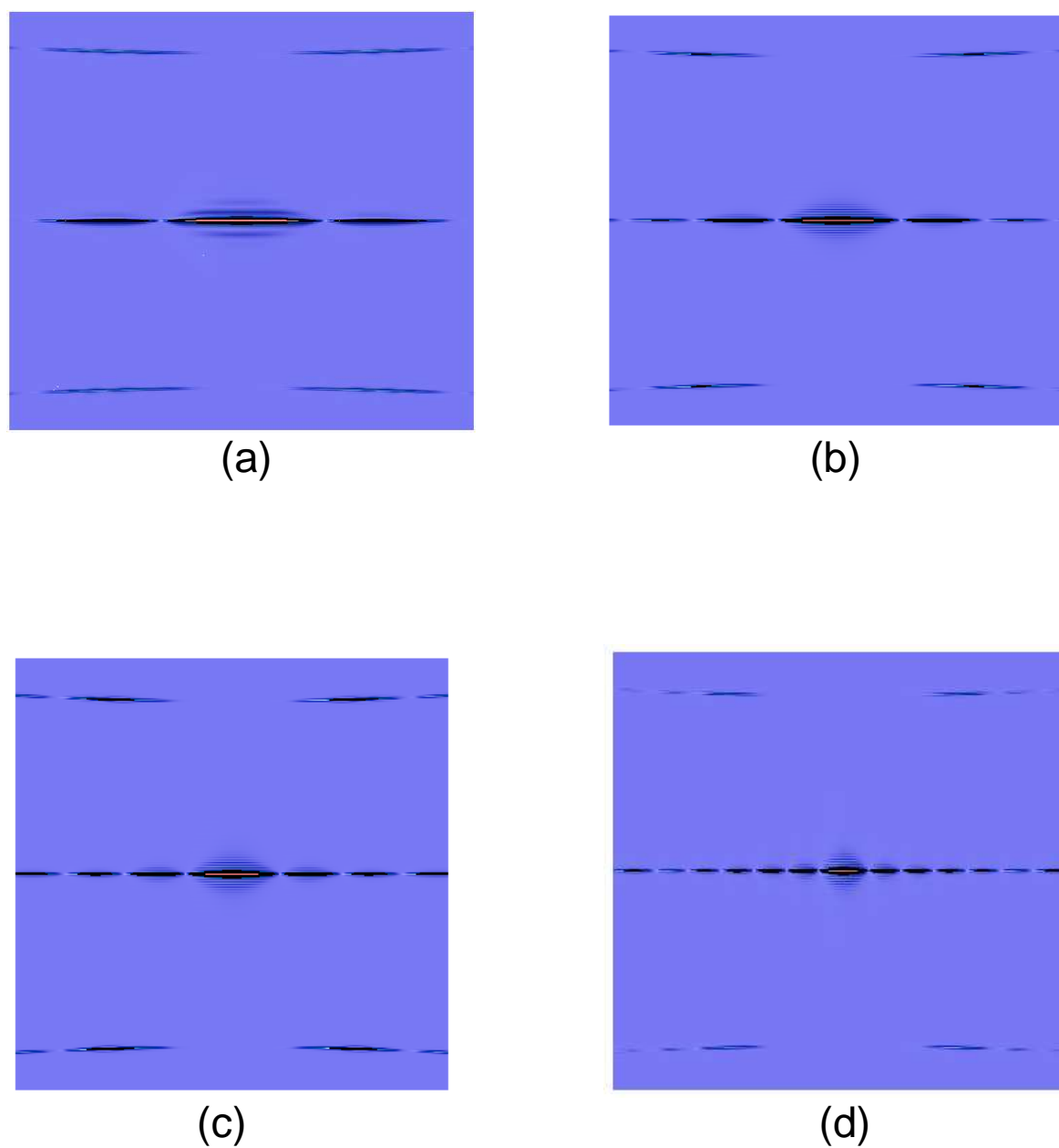


Figure 3. The effect of changing the tube diameter: (a) CNT of type (3,3), $D = 0.4$ nm, (b) type (4,4), $D = 0.6$ nm, (c) type (5,5), $D = 0.7$ nm, (d) type (10,10), $D = 1.4$ nm.

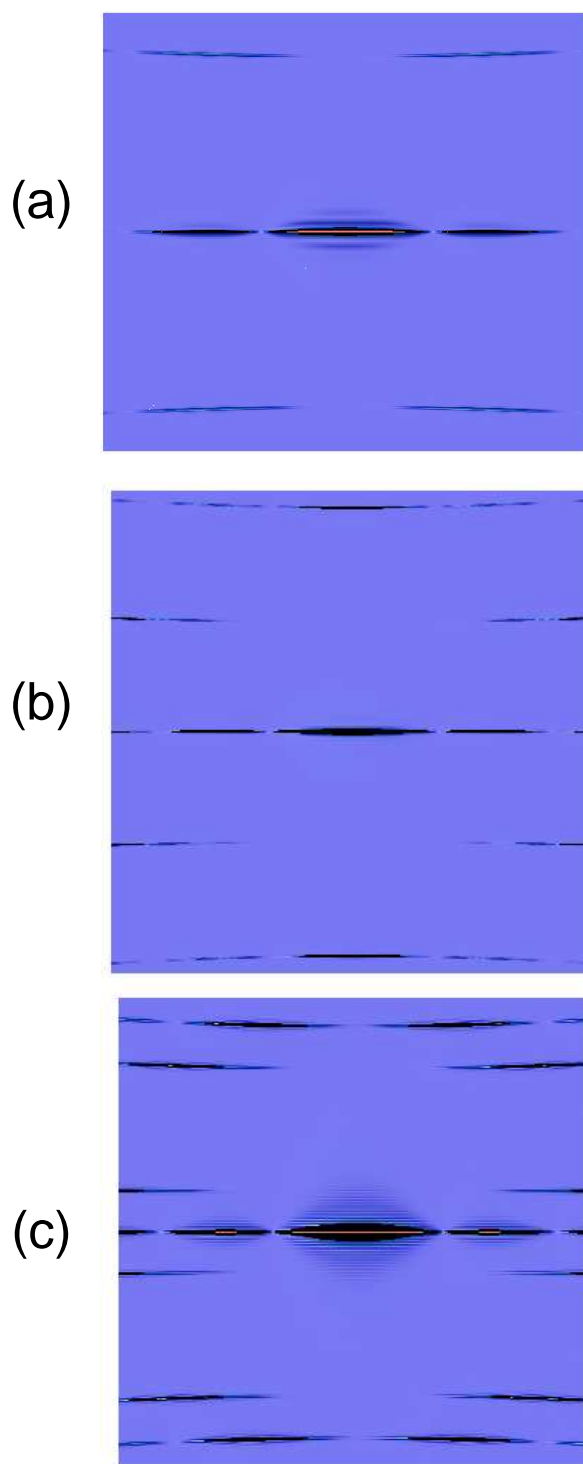


Figure 4. The dependence of XRD patterns on the tube type: (a) armchair (3,3); (b) zig-zag (5,0); (c) chiral (4,2).

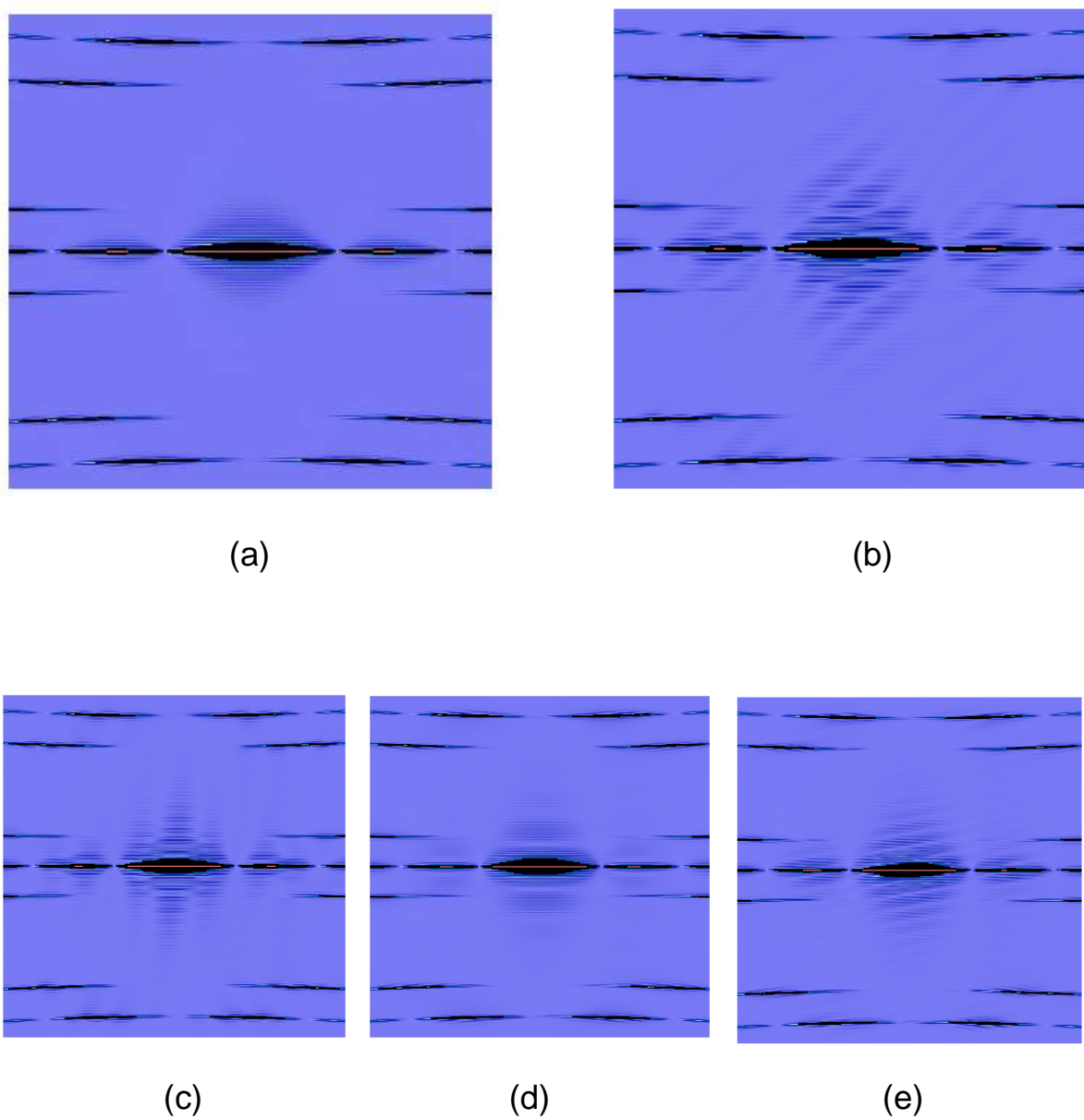


Figure 5. X-ray diffraction from (a) chiral (4,2) nanotube, (b) the same CNT with one Au atom adsorbed to the side at $z = 0$, (c) Au atom attached half-unit cell higher, (d) Au atom attached to the top of CNT, (e) Au atom attached to the side of CNT near its top.